Modal reduction of an advection-diffusion model using a branch basis

Frédéric Joly, Olivier Quéméner, Alain Neveu

MODAL REDUCTION OF AN ADVECTION-DIFFUSION MODEL USING A BRANCH BASIS

F. Joly, O. Quéméner, and A. Neveu
Laboratoire de Mécanique et d'Energétique d'Evry, Courcouronnes, Evry, France

We propose an original method to reduce an advection-diffusion model in which parameters, as well as boundary conditions, are time-dependent. This modal method uses a branch basis, which differs from the Fourier one by a Steklov boundary condition. The treated application is a disk rotating at a variable velocity, with time-dependent volume and superficial thermal inputs. Comparison between the detailed model and the reduced one gives a gain in compu-tational time of 24 times with a maximal error of less than 10%, opening the way to real-time simulation.

1. INTRODUCTION

Numerical resolution of advection-diffusion equations is an active field of research, for thermal engineering of course, but also for other, less usual topics such as financial analysis (see, for example, [1]). There are several ways to solve these equations. For some simple configurations, such as a rotating disk, analytical solutions exist [2]. Analytical solutions present the advantage of being fast and exact, but, unfortunately, they have disadvantage of being nonexistent for 99% of configurations!

Direct numerical simulation consists of discretizing the computation domain on a grid, and searching for the solution $T(M)$ on the nodes of this grid. To have the appropriate precision, the mesh has to be refined, leading to a very large number of unknowns, i.e., a very large computation time. For real-time process command or parametric study, these techniques seem inappropriate, and one has to think about a way to reduce the number of unknown while keeping the main dynamics of the system.

Among the ways to reduce the number of unknowns are modal methods (see, for instance, [3]). Originally used by Fourier himself to solve the 1-D transient conduction equation [4], modal methods consist of searching for the solution as a superposition of elementary functions: $T(M,t) = \Sigma_{i=0}^{\infty} \alpha_i(t) V_i(M)$. The functions $V_i(M)$ are called modes, the set of the functions a base, and the unknown coefficients $\alpha_i(t)$ the states. Of course, in practice, the sum does not go to infinity, but to a number N_{red}. If the number N_{red} of modes necessary to approach the solution with the needed precision is small, then this last method is an appropriate candidate for the above-mentioned applications. The choice of the base is a determinant parameter

Address correspondence to Frédéric Joly, Laboratoire de Mécanique et d'Energétique d'Evry, 40 rue du Pelvoux, CE1455 Courcouronnes, 91020 Evry Cédex, France. E-mail: f.joly@iut.univ-evry.fr

NOMENCLATURE

Bi	Biot number [Eq. (2)]
C_0	volumic capacity
$E(M)$	branch eigenspace
h	convective exchange coefficient
k_0	conductivity
Pe	Péclet number [Eq. (2)]
P_v	heat source
R	disk radius
$T(M)$	temperature field
U	velocity
$V(M)$	branch eigenmode
$W(M)$	modified branch mode
α	branch mode state
ϵ_{max}	maximum error
ϵ_{mean}	averaged-in-space error
ζ	Steklov number
λ	branch eigenvalue
π	dimensionless volume heat source
σ	eigenvalue real part
ϖ	eigenvalue imaginary part

Superscripts

$\star$	adjoint
$-$	complex conjugate

for the quality of the approximation. The modal identification method has been used by Petit et al. [5] to build a modal base using experimental data, and Giraud et al. [6] used such a base to identify a heat flux in a convective 2-D plane channel. Recently, Balima et al. [7] modified the reduced model formulation to build a reduced model for heat conduction with radiative (i.e., nonlinear) boundary conditions. The Karhunen-Loéve expansion (also known as POD) is also an interesting alternative to obtain a basis for high-order systems and can be applied to nonlinear systems. This technique has been widely used in fluid mechanics (see, for example, [8]), but has also been used to build reduced models for thermal systems [9]. However, these two techniques need a knowledge of a detailed model, experimental or numerical, to extract the modes, which is not always feasible.

Another way to build the base is to rely on the heat equation to obtain a generalized eigenvalue problem. "Classical" eigenvalue problems are Dirichlet (the eigenfunction's value is set to zero on the boundary), or Fourier (the ratio between the eigenfunction and its gradient on the boundary is fixed). The eigenmodes satisfying these problems form a base [10] on the domain, but not on the boundary. Unfortunately, the solutions cannot always be decomposed on such a base, especially if the boundary conditions are not homogeneous. This problem has been so far overcome by considering that the temperature field is the sum of two contributions: one "dynamic," satisfying the homogeneous boundary conditions, and thus expandable in terms of the eigenfunctions, and its complement, called the "sliding" contribution. However, only linear problems having the same kind of boundary conditions can be solved using this approach [13]. El Khoury and Neveu [11] applied this technique to the advection-diffusion problem, and showed that the transport term leads to a non-self-adjoint problem. Quéméner et al. [12] successfully used Fourier modes to identify the heat flux obtained by the dry sliding of a pin to the periphery of a rotating disk. In order to solve self-adjoint nonlinear problems associated with nonlinear boundary conditions, Neveu et al. [14] successfully used "branch modes." The originality of the branch modes (named after their first utilization in mechanical engineering) is that the "branch eigenvalue problem" uses a Steklov boundary condition, a boundary condition that depends on the eigenvalue. The Steklov boundary condition yields a basis on the domain and on the boundary. Quéméner et al. [16]

used these modes to solve a conduction problem in which parameters and boundary conditions were highly nonlinear.

In the present article, the same technique is used, but applied to an advection-diffusion problem. The advection term leads to a non-auto-adjoint system in which the operators are not symmetric, which leads to complex eigenmodes. This article is organized as follow. In a first part, the branch problem for a non-self-adjoint problem is defined and its main properties are described. The numerical methods used to solve the problem are then presented. An example of application is given. This simple example admits an analytical solution which gives useful information regarding the branch modes, and a full analysis is given. Finally, the branch modes are used to solve a time-dependent problem, and this reduced model is compared to the detailed one.

2. THE BRANCH MODES OF A THERMAL PROBLEM WITH ADVECTION

Let Ω be a closed domain, solid or fluid, of volumic capacity C_0 and conductivity k_0, delimited by its closed boundary Γ, and animated by a macroscopic movement of velocity $\vec{U}$. Ω is heated by its boundary according to a convective coefficient h_0 and an external temperature T_f, and by a heat source P_v inside its boundary. Characteristic scales being ΔT for temperature, L for length, $||\vec{U}||$ for velocity, $c_0 L^2/k_0$ for time, and $k_0 \Delta T/L^2$ for heat source, the dimensionless heat equation is expressed as

$$\begin{cases} \forall M \in \Omega \quad -\nabla^2 T + \mathrm{Pe}\vec{U} \cdot \vec{\nabla} T = -\dfrac{\partial T}{\partial t} + \pi & (a) \\ \forall M \in \Gamma \quad \vec{\nabla} T \cdot \vec{n} = \mathrm{Bi}(T_f - T) & (b) \end{cases} \tag{1}$$

This equation is governed by three dimensionless control parameters, the Péclet number, the Biot number, and the volume dimensionless heat source, given by

$$\mathrm{Pe} = \frac{C_0 ||\vec{U}|| L}{k_0} \quad \mathrm{Bi} = \frac{L h_0}{k_0} \quad \pi = \frac{P_v L^2}{k_0 \Delta T} \tag{2}$$

respectively.

The definition of the branch modal eigenvalue problem with advection is

$$\begin{cases} \forall M \in \Omega \quad -\nabla^2 V + \mathrm{Pe}\vec{U} \cdot \vec{\nabla} V = \lambda V & (a) \\ \forall M \in \Gamma \quad \vec{\nabla} V \cdot \vec{n} = \lambda \zeta V & (b) \end{cases} \tag{3}$$

where λ and V are, respectively, the eigenvalues and the eigenfunctions of the branch modal basis. The parameter ζ is a numerical parameter called the dimensionless Steklov number. In the dimensional form, the Steklov number ensures that the eigenvalue λ has the same dimension in Eqs. (3*a*) and (3*b*).

As this model is non-self-adjoint, its eigenmodes do not form an orthogonal set, and the adjoint branch modal basis has to be defined:

$$\begin{cases} \forall M \in \Omega \quad -\nabla^2 V^\star - \mathrm{Pe}\vec{U} \cdot \vec{\nabla} V^\star = \lambda V^\star & (a) \\ \forall M \in \Gamma \quad \vec{\nabla} V^\star \cdot \vec{n} = \lambda \zeta V^\star & (b) \end{cases} \tag{4}$$

The set of functions $(V_i, V_i^\star)$ forms a biorthogonal system, and verifies the following orthogonality property:

$$\langle \overline{V}_i^\star, V_j \rangle = \int_\Omega \overline{V}_i^\star(M) V_j(M) d\Omega + \int_\Gamma \zeta \overline{V}_i^\star(M) V_j(M)\, d\Gamma = \delta_{ij} \tag{5}$$

The subscript denotes the order of the eigenmode, $\delta_{i,j} = 1$ if $i = j$ and $\delta_{i,j} = 0$ otherwise, $\langle ., . \rangle$ is the inner product, and $\overline{V}_i^\star$ is the complex conjugate of $V_i^\star$. Any function can be decomposed as

$$T(M,t) = \sum_{i=0}^{\infty} \alpha_i(t) V_i(M) \tag{6}$$

where $V_i(M)$ are the branch modes defined by Eq. (3), and α_i are the unknown coefficients named hereafter states.

Equation (3*b*) represents the main particularity of the branch modal basis. For a classical modal method, the boundary condition corresponds to the associated physical problem [Eq. (1*b*)], and a Fourier boundary condition is obtained:

$$\begin{cases} \forall M \in \Omega & -\nabla^2 V + \mathrm{Pe}\vec{U} \cdot \vec{\nabla} V = \lambda V \quad (a) \\ \forall M \in \Gamma & \vec{\nabla} V \cdot \vec{n} = \mathrm{Bi}_0 V \quad (b) \end{cases} \tag{7}$$

This classical modal basis imposes the convective coefficient value Bi_0 in the boundary condition. For a physical problem characterized by a time-dependent boundary condition, $\mathrm{Bi}(t) \neq \mathrm{Bi}_0$ [Eq. (1*b*)], it is impossible to rebuild the thermal flux density at the boundary [15]. Such a modal basis is then not adapted to time-dependent boundary conditions or nonlinear thermal problem. On the other hand, the branch modal basis defined by Eq. (3) is not linked to a specific physical boundary condition. Because of the λ eigenvalue presence, such a boundary condition allows one to rebuild temperature and thermal flux density for all Bi convective coefficient. This basis is then adapted to nonstationary and nonlinear thermal problems.

3. NUMERICAL METHODS

3.1. Spatial Discretization

The usual weak formulation of Eq. (1) yields

$$\int_\Omega \vec{\nabla} T \cdot \vec{\nabla} g\, d\Omega + \mathrm{Pe} \int_\Omega \vec{U} \cdot \vec{\nabla} T g\, d\Omega + \mathrm{Bi} \int_\Gamma T g d\Gamma = \int_\Omega \left(-\frac{\partial T}{\partial t} + \pi \right) g\, d\Omega + \mathrm{Bi} \int_\Gamma T_f g\, d\Gamma \tag{8}$$

Temperature is defined in the space $H^1(\overline{\Omega})$, and g are test functions defined in $H^1(\overline{\Omega})$. The eigenspace $H^1(\overline{\Omega})$ is defined by $H^1(\overline{\Omega}) \equiv H_0^1(\Omega) \times H^{1/2}(\Gamma)$.

The weak formulation of the eigenvalue problem and its adjoint reads

$$\begin{cases} \displaystyle\int_\Omega \vec{\nabla} V_i \cdot \vec{\nabla} g \, d\Omega + \int_\Omega \mathrm{Pe}\vec{U} \cdot \vec{\nabla} V_i g \, d\Omega = -\lambda_i \left(\int_\Omega V_i \, g d\Omega + \int_\Gamma \zeta V_i g \, d\Gamma \right) \\ \displaystyle\int_\Omega \vec{\nabla} V_i^* \cdot \vec{\nabla} g \, d\Omega - \int_\Omega \mathrm{Pe}\vec{U} \cdot \vec{\nabla} V_i^* g \, d\Omega = -\lambda_i \left(\int_\Omega V_i^* g \, d\Omega + \int_\Gamma \zeta V_i^* g \, d\Gamma \right) \end{cases} \tag{9}$$

The term $\int_\Omega V_i g \, d\Omega$ refers to the Dirichlet modes, i.e., volume modes, while the term $\int_\Gamma \zeta V_i g \, d\Gamma$ refers to the Steklov modes, i.e., superficial modes. The Steklov parameter balances these two terms: $\zeta = 0$ gives the Dirichlet modes, while $\zeta \to \infty$ gives the Steklov modes. In order to have a similar contribution of both families, and to have a basis with volume and superficial modes, $\zeta \approx 1$. Furthermore, it has been proven in the self-adjoint case that $\zeta = 1$ is effectively the best value [16].

The following operators are then defined:

$$\begin{cases} \mathbb{K} = \int_\Omega \vec{\nabla} \cdot \vec{\nabla} g \, d\Omega & \mathbb{F}_\mathrm{O} = \int_\Gamma \mathrm{Bi} \cdot g \, d\Gamma \\ \mathbb{S}_\mathrm{surf} = \int_\Gamma \mathrm{Bi} \, T_f g \, d\Gamma & \mathbb{S}_\mathrm{vol} = \int_\Omega \pi g \, d\Omega \\ \mathbb{C}_\mathrm{surf} = \int_\Gamma \zeta \cdot g \, d\Gamma & \mathbb{C}_\mathrm{vol} = \int_\Omega g \, d\Omega \\ \mathbb{T} = \int_\Omega \mathrm{Pe} \, \vec{U} \cdot \vec{\nabla} \cdot g \, d\Omega \end{cases} \tag{10}$$

They are discretized on an order 1 finite-element basis, leading to unsymmetrical matrices. For large Péclet numbers (i.e., $\mathrm{Pe} \approx 5{,}000$), the convection operator $\mathbb{T}$ is regularized using SUPG regularization [17]. The velocity field is computed separately and is a datum of the problem.

3.2. Numerical Resolution of the Branch Problem

With the operators defined in Eq. (10), the branch problem and its adjoint are respectively defined by

$$\begin{cases} [\mathbb{K} + \mathbb{T}] V_i = -\lambda_i (\mathbb{C}_\mathrm{vol} + \mathbb{C}_\mathrm{surf}) V_i \\ [\mathbb{K} - \mathbb{T}] V_i^* = -\lambda_i (\mathbb{C}_\mathrm{vol} + \mathbb{C}_\mathrm{surf}) V_i^* \end{cases} \tag{11}$$

Those generalized eigenvalue problems are solved after spatial discretization via a slight modification of routine dndrv6.f of the Arpack package. This software is based on an algorithmic variant of the Arnoldi process called the Implicitly Restarted Arnoldi Method (IRAM)(for more information about Arpack, see [18]). The spatial discretization leads to a finite number of modes N_mesh equal to the number of mesh nodes, and eigenfunctions become eigenvectors of dimension N_mesh.

As the operators are non-self-adjoint, the eigenmodes are complex, and the corresponding states α_i are complex too. The manipulation of complex eigenmodes is not a fundamental difficulty. Nevertheless, the numerical treatment could become painful, and the physical explanation of the eigenvectors is more delicate. Moreover, the temperature field is real, and so this "real" property should be exploited in order to simplify the computations. The eigenvectors come by couple $(V_k, \overline{V}_k)$, where $\overline{V}_k$ is

the conjugate of V_k. Each couple generates a subeigenspace E_k, associated to the eigenvalue λ_k. This subeigenspace is of dimension 2 if λ_k is complex and of dimension 1 otherwise. Subeigenspaces are orthogonal ($\forall i,k \in \mathbb{N} \quad E_i \perp E_k$). A new basis is introduced with vectors defined by

$$W_k^{\Re} = \frac{2}{\sqrt{2}}\Re(V_k) \quad W_k^{\Im} = -\frac{2}{\sqrt{2}}\Im(V_k) \tag{12}$$

Of course, a real eigenvector is not modified. It is important to notice that these new vectors are not eigenvectors, as they do not verify the eigenvalue problem (11), but

$$[\mathbb{K}+\mathbb{T}]W_i^{\aleph_1} = \sigma_i(\mathbb{C}_{\text{vol}}+\mathbb{C}_{\text{surf}})W_i^{\aleph_1} + (-1)^{\delta_{\aleph_1\Re}}\varpi_i(\mathbb{C}_{\text{vol}}+\mathbb{C}_{\text{surf}})W_i^{\aleph_2}$$

with $\lambda_i = \sigma_i + j\varpi_i$, and if $\aleph_1 = \Im$ (or $\Re$), $\aleph_2 = \Re$ (or $\Im$).

However, as a linear combination of $(V_k, \overline{V}_k)$, $(W_k^{\Re}, W_k^{\Im})$ also generates a basis for E_k, and the couples $\{(W_k^{\Re}, W_k^{\Im}), (W_k^{\Re *}, W_k^{\Im *})\}$ still form a biorthonormal basis verifying the following orthogonality property:

$$\langle W_i^{\aleph_1}, W_j^{*\aleph_2}\rangle = \delta_{ij}\delta_{\aleph_1\aleph_2} \tag{13}$$

In the old formulation, an eigenvector $V_i = \Re(V_i) + i\Im(V_i)$ is followed by its conjugate $V_{i+1} = \overline{V}_i = \Re(V_i) - i\Im(V_i)$. For reasons of simplicity, in the new formulation, $W_i^{\Re}$ will be noted W_i, $W_i^{\Im}$ being noted W_{i+1}. This way, the temperature field will still be decomposed as $T(M) = \Sigma_{i=0}^{N}\alpha_i W_i(M)$, but this time with α_i and W_i real. However, the eigenvalues λ_k associated to the subeigenspaces E_k are still complex.

3.3. Numerical Resolution of the Evolution Equation

3.3.1. The detailed model. With the notations defined in Eq. (10), Eq. (8) becomes

$$(\mathbb{K}+\mathbb{F}_{\text{O}}+\mathbb{T})T = -\mathbb{C}_{\text{vol}}\frac{\partial T}{\partial t} + (\mathbb{S}_{\text{vol}}+\mathbb{S}_{\text{surf}}) \tag{14}$$

Temperature is evolved after spatial discretization in time via an implicit first-order Euler scheme with adaptive time steps. The resulting linear system is solved by a preconditioned BICGSTAB algorithm designed for sparse matrices [19].

3.3.2. The reduced model. In Eq. (8), the temperature field is replaced by its modal decomposition [Eq. (6)], while the test functions g are the adjoint branch problem eigenmodes:

$$\sum_{j=0}^{\infty} W_j^*(\mathbb{K}+\mathbb{F}_{\text{O}}+\mathbb{T})W_i\alpha_i = -\sum_{j=0}^{\infty} W_j^*\mathbb{C}_{\text{vol}}W_i\frac{\partial\alpha_i}{\partial t} + \sum_{j=0}^{\infty} W_j^*(\mathbb{S}_{\text{vol}}+\mathbb{S}_{\text{surf}}) \tag{15}$$

As the eigenproblem is discretized on a mesh with N_{mesh} nodes, only N_{mesh} eigenmodes are accessible. The above equation should then be written as

$$\sum_{j=0}^{N_{\text{mesh}}} W_j^*(\mathbb{K}+\mathbb{F}_{\text{O}}+\mathbb{T})W_i\alpha_i = -\sum_{j=0}^{N_{\text{mesh}}} W_j^*\mathbb{C}_{\text{vol}}W_i\frac{\partial\alpha_i}{\partial t}+\sum_{j=0}^{N_{\text{mesh}}} W_j^*(\mathbb{S}_{\text{vol}}+\mathbb{S}_{\text{surf}}) \quad (16)$$

This equation is the complete modal state equation, and is not reduced. The matrices $\Sigma_{j=0}^{N_{\text{mesh}}} W_j^*\mathbb{C}_{\text{vol}}W_i$ and $\Sigma_{j=0}^{N_{\text{mesh}}} W_j^*(\mathbb{K}+\mathbb{F}_{\text{O}}+\mathbb{T})W_i$ are square matrices of order N_{mesh}, i.e., of the same dimension as the detailed model. More than that, from a numerical point of view, this equation is more difficult to solve than the detailed model: the matrices of the detailed model are sparse, and designed algorithms exist to exploit this property. On the other hand, matrices of a modal system are full. It is then mandatory to reduce the number of unknown (i.e., eigenmodes) to solve this equation and to save computation time as well as memory. The reduction consists of finding (and keeping) the N_{red} most important modes, allowing one to reproduce the dynamics of the system. To be efficient in terms of computation time and memory, one must have $N_{\text{red}} << N_{\text{mesh}}$. The key of the problem is to find a criterion able to determine which are the most important modes. To do so, several algorithms exist. The algorithm we use to reduce the model is described in detail later. Finally, the system to solve is

$$\sum_{j=0}^{N_{\text{red}}} W_j^*(\mathbb{K}+\mathbb{F}_{\text{O}}+\mathbb{T})W_i\alpha_i = -\sum_{j=0}^{N_{\text{red}}} W_j^*\mathbb{C}_{\text{vol}}W_i\frac{\partial\alpha_i}{\partial t}+\sum_{j=0}^{N_{\text{red}}} W_j^*(\mathbb{S}_{\text{vol}}+\mathbb{S}_{\text{surf}}) \quad (17)$$

The states are also evolved in time via an implicit first-order Euler scheme with adaptive time steps, but the linear system is solved by a LU algorithm.

4. EXAMPLE OF APPLICATION: THE ROTATING DISK

The chosen configuration to illustrate the branch modes reduction is a disk of radius R, volume capacity C_0, and conductivity k_0, rotating around its axis at an angular velocity ω. This disk can be heated by a heat flux P_v on its subdomain Ω_2 and exchange heat by its boundaries (see Figure 1*a*). With the characteristic scales for length and velocity being R and ωR, respectively, the evolution equation and boundary conditions are given by

$$\begin{cases} \forall M \in \Omega_{1,2} & \frac{\partial T}{\partial t} = \nabla^2 T - \text{Pe}\,\vec{U}\cdot\vec{\nabla}T + \pi_{1,2} \\ & \pi_1 = 0 \quad \pi_2 = 100 f_1(t) \quad \text{Pe} = 10^5 f_2(t) \end{cases} \quad (18)$$

$$\begin{cases} \forall M \in \Gamma_{1,3} & \vec{\nabla}T = 0 \\ \forall M \in \Gamma_2 & \vec{\nabla}T = \text{Bi}(T_{f2} - T) \quad \text{Bi} = 10[1+f_2(t)] \quad T_{f1} = 1 \\ \forall M \in \Gamma_4 & \vec{\nabla}T = \text{Bi}(T_{f1} - T) \quad \text{Bi} = 10[1+f_2(t)] \quad T_{f2} = -1 \end{cases} \quad (19)$$

the functions $f_{1,2}(t)$ being described in Figure 1*b*.

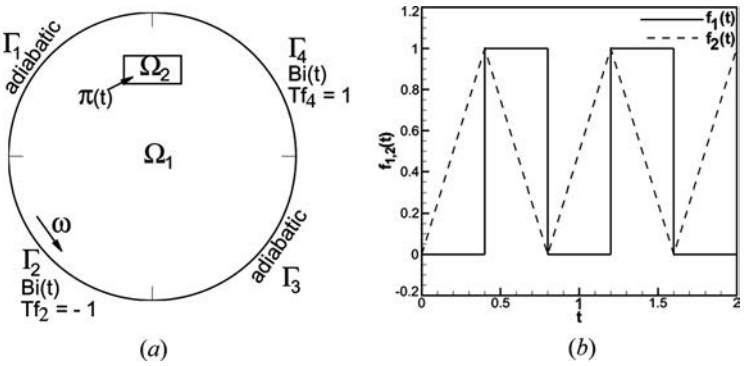

Figure 1. Physical model (*a*) and temporal evolution of the thermal inputs (*b*).

4.1. Mesh Size

As the domain can be subjected to superficial and volume thermal inputs, the choice of a uniform mesh has been made. In this article two aspects are compared:

1. Computation time between the detailed and reduced models. In order not to falsify results, care must be taken not to have an unnecessary large mesh.
2. Temperature field of the detailed and reduced models, and the loss of precision that occurs from using the reduced models. For this comparison to make sense, the detailed model has to be precise enough to be a reference.

A compromise has then to be made between a refined grid with good precision but a computation time forbidding comparison with the reduced model, and a small grid leading to imprecise results. A sensitivity analysis has been carried out. Table 1 shows the relative error of the temperature maximum between the current mesh and a mesh with 14,945 nodes for different meshes,

$$\epsilon = \frac{T_{\max}(N_{\text{mesh}}) - T_{\max}(N_{\text{mesh}} = 14{,}945)}{T_{\max}(N_{\text{mesh}} = 14{,}945) - T_{\min}(N_{\text{mesh}} = 14{,}945)}$$

The test case is $\text{Pe} = 10^5$, $\text{Bi} = 10$, $T_{\max} = 1$, and $T_{\min} = -1$. Table 1 shows that to have a converged result (error less than 1%), a mesh with 9,498 nodes is required. However, this level of refinement is not necessary, and this grid leads to a computation time too large to be honestly compared with the reduced models. On the other hand, a grid with $N_{\text{mesh}} = 1{,}079$ nodes leads to as error of 25%, which

Table 1. Relative error of the temperature field maximum as a function of the mesh size

N	1,079	3,134	4,785	9,498
ϵ(%)	24.2	4.5	2.6	0.2

forbids any comparison with the reduced models. The grid 4,785 is an acceptable compromise, and all computations have been done on this grid.

In order to validate our code, the detailed model has been compared with computations done by COMSOL Multiphysics [20], for different meshes and various Péeclet and Biot numbers. The maximum difference between our code and COMSOL Multiphysics was 1.6%.

5. THE BASIS MAIN PROPERTIES

For this problem an analytical solution can be sought of (details are given in the Appendix). This analysis reveals that the main structure of the base does not depend on the Péclet number. The eigenmodes depend on two integers n and m, and a more natural notation appears:

$$\begin{cases} \lambda_{n,m} = -(a_{n,m}^2 - b_{n,m}^2) + j(2|a_{n,m} \cdot b_{n,m}| - n\,\mathrm{Pe}) \\ V_{n,m}(\rho,\theta) = A_{n,m} \cdot J_n(\alpha_{n,m} \cdot \rho) \cdot e^{j \cdot n \cdot (\theta + \phi_{n,m})} \end{cases} \tag{20}$$

$\lambda_{n,m} = \bar{\lambda}_{-n,m}$ are the eigenvalues and are depicted on the left side of Figure 2 in the $(\Re(\lambda_i), \Im(\lambda_i))$ plane for a basis computed at $\mathrm{Pe} = 10$. $V_{n,m} = \overline{V}_{-n,m}$ are the eigenvectors and are defined by n, the azimuthal periodicity, and m, the radial one. We proceed to a change of basis as described in Section 3.2, and redefine $W_{n,m} = (2/\sqrt{2})\Re(V_{n,m})$ and $W_{-n,m} = -(2/\sqrt{2})\Im(V_{n,m})$. $W_{n,m}$ and $W_{-n,m}$ have the same radial and azimuthal periodicities and differ only by a rotation. It is important to notice that any eigenvector

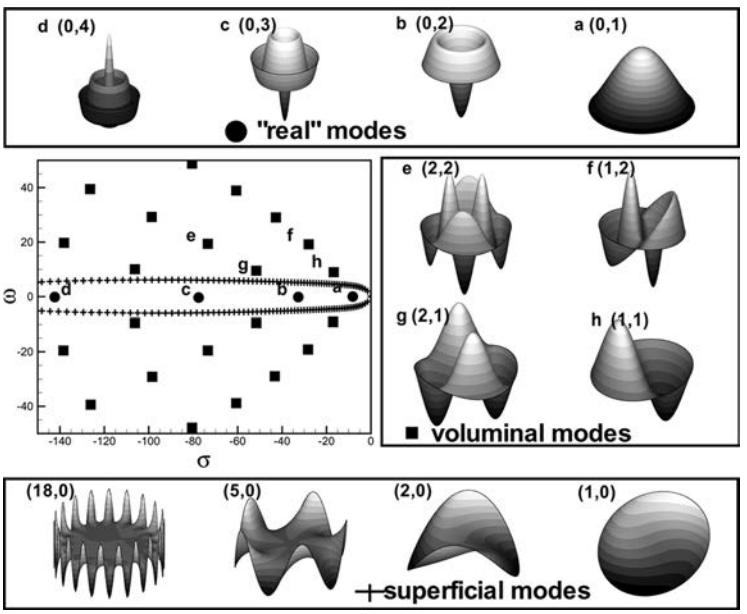

Figure 2. Eigenvalues spectrum for $\mathrm{Pe} = 10$.

$W_{n,m}$ is defined modulo a rotation, and only the subspace $E_{n,m} = (W_{n,m}, W_{-n,m})$ is fully defined. Following this notation, the following properties arise.

It is readily seen that axisymmetric modes, with $n = 0$, are real and define subspaces of dimension 1 $E_{0,m}$. Because of their configuration, these modes cannot take into account any transport effect, and are therefore completely independent of the Péclet number. The insert at the top of Figure 2 shows $W_{0,1}$, $W_{0,2}$, $W_{0,3}$, $W_{0,4}$. Their eigenvalues are, of course, on the $\Re(\lambda_i)$ axis, and are depicted by black circles. $E_{0,0}$ is completely flat in the domain and on the border.

$E_{n,0}$ are subspaces for superficial modes. These modes are flat on the domain except near the border and have no radial periodicity. The superficial mode existence is the main property of a branch basis. Such modes, which do not appear in a classical Fourier basis, allow the reconstitution of any boundary condition. Typical examples are given by the insert at the bottom of Figure 2, where $W_{1,0}$, $W_{2,0}$, $W_{5,0}$, $W_{18,0}$ are depicted. The superficial mode eigenvalues are depicted by black crosses.

$E_{n,m}$ with $n \neq 0$ and $m \neq 0$ correspond to the volume and nonaxisymmetric eigenspaces. Their shape and eigenvalue desend on the Péclet number, and their eigenvalue imaginary part behaves as $n \cdot \mathrm{Pe}$, as seen at the left of Figure 2, where their eigenvalues are represented by black squares. $W_{1,1}$, $W_{1,2}$, $W_{2,1}$, $W_{2,2}$ are represented on the right side of Figure 2.

6. REDUCTION STRATEGY

6.1. Basis Selection

Equation (3) shows that for each Péclet number there corresponds a basis. For a problem in which the Péclet number varies strongly, what basis should be used? Following Eq. (6), are all bases equivalent? A criterion to answer this question is to compute the number of modes N_ϵ necessary to approach the detailed solution with an error smaller than ϵ; the smaller N_ϵ, the better the basis. Several bases at different Péclet number were computed, as well as detailed and static temperature fields. These temperature fields were projected on each basis, and we looked at the number of modes necessary to approach the detailed solution with a mean difference between the detailed model and the reduced one of less than 1%. Results are presented in Table 2. As $E_{0,0}$ fixes the mean temperature and is always present in the decomposition, it will not be explicitly specified.

Table 2. Number of modes to approach the detailed model with a mean difference less than 1%

	Detailed model					
Basis	$\mathrm{Pe} = 0$	$\mathrm{Pe} = 1$	$\mathrm{Pe} = 10$	$\mathrm{Pe} = 100$	$\mathrm{Pe} = 10^3$	$\mathrm{Pe} = 10^5$
$\mathrm{Pe} = 0$	31	31	38	35	34	3
$\mathrm{Pe} = 10$	29	31	34	33	30	3
$\mathrm{Pe} = 10^4$	195	253	203	87	21	3

It is readily seen that the bases are not equivalent. A basis computed at a low Péclet number (even at $\mathrm{Pe} = 0$) is able to rebuild a solution at $\mathrm{Pe} \gg 1$, while a basis computed at a large Péclet number is inefficient to rebuild low-Péclet-number temperature fields. For a problem in which the Péclet number varies strongly, the optimum basis appears to be at $\mathrm{Pe} \approx 10$. However, computing a basis at high Péclet number is not useless. A basis is optimally designed to be used at the Péclet at which it has been computed. So, for a problem in which the disk always turns at high speed, it is best to use a large Péclet basis.

6.2. Hierarchy Criterion

Any temperature field $T(M)$ can be decomposed on a branch basis. The order of importance of the subspaces needed to rebuild $T(M)$ is determined as follows. Using the orthogonal property [Eq.(5)], the states are computed by

$$\alpha_i = \overline{W}_i^* (\mathbb{C}_{\mathrm{vol}} + \mathbb{C}_{\mathrm{surf}}) T(M) \tag{21}$$

The larger α_i is, the more the corresponding mode is necessary, yielding a hierarchy criterion more relevant than the time-constant one. Table 3 presents the order of importance of the 10 first subspaces [determined following Eq. (21)] needed to approach the solution $\mathrm{Pe} = 10$ for different bases. A black cell means that the subspace is not among the 10 more important subspaces. The main subspaces are present independent of the chosen basis, and adaptations are due to mode shape, which is modified by the velocity. As a matter of fact, any temperature field solution of an advection-diffusion equation submitted to superficial thermal inputs is characterized by a boundary-layer thickness $\delta_T(\mathrm{Pe})$, a function of the Péclet number. Complex volume modes are also characterized by a boundary-layer thickness $\delta_B(\mathrm{Pe})$, as clearly illustrated by Figure 3, where mode $W_{2,1}$ is depicted for a base computed at $\mathrm{Pe} = 0$ (*a*) and $\mathrm{Pe} = 10^4$ (*b*). The difficulty is then to rebuild a temperature field characterized by δ_T with modes characterized by δ_B. For $\delta_T \neq \delta_B$, complex volume modes characterized by δ_B have to be coupled with modes with a higher periodicity in r in order to rebuild a temperature field characterized by δ_T. This is illustrated in Table 3 for the $\mathrm{Pe} = 10^4$ base, where subspaces $E_{1,2}$ and $E_{1,3}$ are coupled with $E_{1,1}$ to reconstitute the temperature field at Pe=10.

Table 3. Order of importance of the 10 first subspaces needed to approach the solution $\mathrm{Pe} = 10$ for different bases

	Subspaces												
	Superficial					Volume						Real	
Basis	(1,0)	(2,0)	(3,0)	(4,0)	(6,0)	(1,1)	(2,1)	(3,1)	(4,1)	(1,2)	(1,3)	(0,1)	(0,2)
$\mathrm{Pe} = 0$	2	1	6		7	4	9	8	10			3	5
$\mathrm{Pe} = 10$	2	1	6	10	9	4	5	8				3	7
$\mathrm{Pe} = 100$	1	2	8		7	4	5	10		9		3	6
$\mathrm{Pe} = 10^4$	2	1	10		6	4	5			8	9	3	7

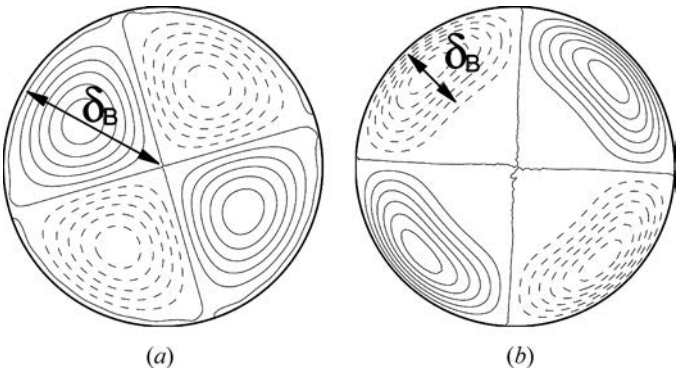

Figure 3. Mode $W_{2,1}$ computed at Pe = 0 (*a*) and Pe = 10^4 (*b*).

6.3. Mode Selection Inside the Selected Basis

The computed basis order being the mesh order, it has to be reduced in order to reduce computation time. The main question is, once the basis is computed, how the relevant modes are selected. The most intuitive way to reduce the base is to use the Marshall truncation [21], e.g., to select modes with the largest time constant. If this method is very simple to write, there is little chance that the resulting reduced basis will be optimized, and a simple look at Figure 2 shows that superficial modes will be overrepresented. We have developed another method, inspired by the snapshot methods (see, for example, [22]). This method has the advantage of being intuitive, easy to write, and almost costless in term of computation time.

A static solution at a given Péclet number is computed (referred to as snapshot).
The resulting temperature field is projected on the basis.
The N_{first} more important subspaces are selected [Eq. (21)]. It is crucial to select the complete subeigenspace; to select a mode without its complex conjugate would lead to an instability.
These three steps are repeated for different value of the Péclet number.
The reduced basis will be the reunion of the different sets of modes, yielding a set of N_{red} modes.

Table 4 shows the more relevant subspaces for snapshots computed at different Péclet numbers. Different types of subspaces appear, depending on the snapshot Péclet number. For small and moderate Péclet numbers, volume and superficial subspaces are necessary for thermal reconstruction. On the other hand, for a large Péclet number (Pe = 10^5), velocity homogenizes the thermal azimuthal evolution, explaining why on the 10 more influent subspaces, six are axisymmetric and only two are superficial. This proves that the different snapshots should contain enough information to be pertinent, and have to cover the range of parameters considered in the physical problem. For the treated application, six snapshots have been considered at Pe = 10^n, with $n = 0$–5.

Table 4. Order of importance of the 10 more important subspaces for a basis computed at Pe = 10 for different snapshots

	Subspaces															
	Superficial						Volume					Real				
snapshot	(1,0)	(2,0)	(3,0)	(4,0)	(5,0)	(6,0)	(1,1)	(2,1)	(3,1)	(1,2)	(1,3)	(0,1)	(0,2)	(0,3)	(0,4)	(0,6)	(0,7)
Pe = 0	2	1	6	8	10	9	3	5	7			4					
Pe = 10	2	1	6	10		9	4	5	8			3	7				
Pe = 10^3	2	4	7		10		5			6	9	1	3		8		
Pe = 10^5	4	10					8			9		1	2	7	3	5	6

7. REDUCED-MODEL UTILIZATION

In this section the detailed model is compared with different reduced models for the temporal simulation described in section 4. Table 5 shows various errors, the computation times for various reduced models, as well as an indication about the memory used by the computer.

The number of modes is investigated first. An eigensubspace can be of dimension 1 or 2, and it is impossible to determine the number of unknowns and the memory requirements from the number of subspaces selected. That is why the number of modes is given instead of the number of subspaces. The number of subspaces kept by snapshot is imposed, as well as the number of snapshots. However, one or several subspaces can appear in the N_{first} most important subspaces of several snapshots, as shown by Table 4, where subspaces (1,0), (2,0), (1,1), and (0,1) appear for every snapshot, leading to a final number of subspaces different from $N_{\text{first}} \times N_{\text{snapshot}}$. However, it is seen that the total number of modes (and not subspaces) tends to $2N_{\text{first}}$ when N_{first} is large; i.e., the number of total subspaces is almost the number of subspaces kept by snapshot. This tends to indicate that if N_{first} is large enough (≈ 50), the N_{first} most important modes are the same whatever the value of the Péclet number used to compute the snapshot, and only their order of appearance changes in this subspace. The number of modes allows computing the size of the operators, and thus gives an indication about the memory used by the computer.

Table 5. Comparisons between the detailed model and the reduced ones

	Detailed model	Reduced models							
N_{first}		5	10	20	30	40	50	60	80
N_{red}		10	22	47	74	88	104	120	160
$\epsilon_{\max}$ (%)		25	15	17	12	11	9	7	5
$\langle\epsilon_{\max}\rangle$(%)		4.5	4.3	3.3	2.7	2.7	2.5	2.4	2.4
ϵ_{mean}(%)		3.9	2.7	1.4	1.1	1.0	1.0	1.0	1.0
$\langle\epsilon_{\text{mean}}\rangle$(%)		0.6	0.6	0.6	0.4	0.4	0.4	0.4	0.4
$t_{\text{CPU}}(s)$	27,160.6	37	55	175	492	743	1,143	1,760	5,040
Gain in time	1	730	490	155	55	37	24	15	5
Operator size	33,105	100	484	2,209	5,476	7,744	10,816	14,400	25,600
Gain in memory	1	331	69	15	6	4.3	3	2.3	1.3

The size of the operators is the number of nonzero values in each matrix representing an operator. In the detailed model, those matrices are sparse, and the number of nonzero coefficients is not $N_{\text{mesh}} \times N_{\text{mesh}}$ but around $7N_{\text{mesh}}$, while the matrices representing the operators of modal model are full, thus of size $N_{\text{red}} \times N_{\text{red}}$, explaining why, although the number of unknown is decreased from 4,785 to 160, there is almost no reduction in terms of used memory.

The lost of accuracy generated by the use of a modal model is now studied. $\epsilon_{\max}$ is the maximum of the error during the simulation, defined by

$$\epsilon_{\max} = \frac{\max_{\forall t}[\max_{\forall x} |T_d(x,t) - T_r(x,t)|]}{max_{\forall t,x}[T_d(x,t) - \min_{\forall t,x} T_d(x,t)]} \tag{22}$$

where T_d is the temperature field given by the detailed model and T_r is the temperature given by the reduced one. $\langle \epsilon_{\max} \rangle$ is the temporal mean of $\epsilon_{\max}$, ϵ_{mean} is the maximum during the simulation of the spatially averaged error, while $\langle \epsilon_{\text{mean}} \rangle$ is the error averaged in time and space.

We notice first that to have a maximal error $\epsilon_{\max} < 10\%$ during the entire simulation, 104 modes are needed, leading to a computation-time gain of 24 times and a gain of 3 times in term of computer memory. This gain takes into account the computational time to select the modes. Figure 4 shows the maximal error during the simulation for different reduced models. Independent of the number of modes, the errors are located near $t = 0.8$ and $t = 1.6$, when the thermal input variations

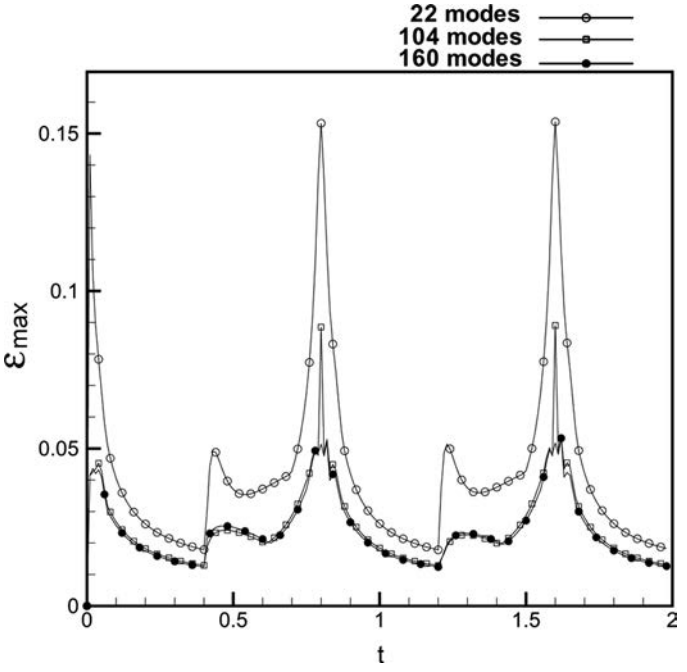

Figure 4. Maximal error evolution of different reduced models.

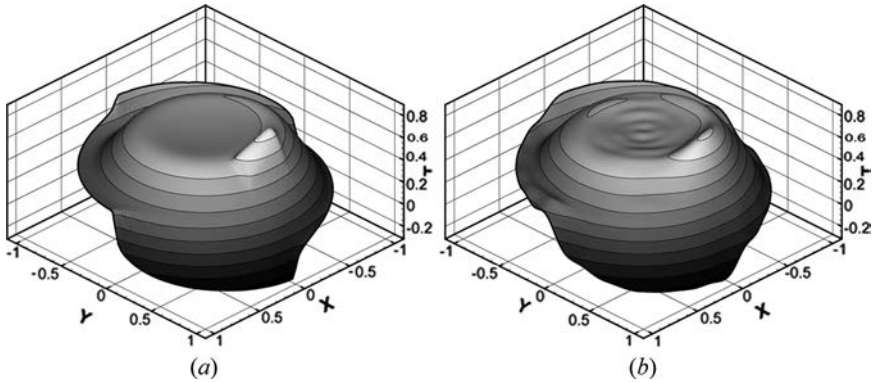

Figure 5. Temperature fields at $t = 1.60$ for (a) the detailed model and (b) the reduced one with $N_{\text{red}} = 104$.

are very stiff and discontinuous. It is important to notice that the only major difference between the $N_{\text{red}} = 104$ model and $N_{\text{red}} = 160$ is at $t = 0.8$ and $t = 1.6$, where the error stays below 5% for $N_{\text{red}} = 160$ while it goes to 9% for $N_{\text{red}} = 104$. The fact that the error is located in time is also shown by the low value of $\langle \epsilon_{\max} \rangle$, which is 2.5% for $N_{\text{red}} = 104$ and a computation-time gain of 24, and of 2.4% for $N_{\text{red}} = 160$ 160 and computation-time gain of 5. Moreover, the error is located in space, as is proven by ϵ_{mean}, the maximum of the spatially averaged error, which is of the order of 1% for a computation-time gain of 24.

This last point is clearly illustrated by Figure 5, showing the temperature fields at $t = 1.6$, i.e., when the error is maximum. Figure 5a represents the exact solution, while Figure 5b represents the reduced model with $N_{\text{red}} = 104$. Despite the complexity of this temperature field, the reduced model catches the volume and superficial thermal loads and rebuilds the temperature correctly.

Figure 6 depicts temperature fields computed by the detailed model (left) and by the $N_{\text{red}} = 104$ reduced one (right) just after $t = 1.6$ change of slope of the thermal inputs, that is, $t = 1.600$ (a and b), $t = 1.604$ (c and d), and $t = 1.606$ (e and f). This exemplifies that the reduced model can respond to stiff inputs, and that even at a very small time scale, hot-spot dynamics are conserved, as well as superficial dynamics.

8. CONCLUSION

In this article, branch modes for an advection-diffusion problem have been computed and have been used to build a reduced model. The branch basis structure in a simple geometry has been fully analyzed, revealing more general properties such as the existence of volume and superficial modes. The existence of superficial modes allows one to rebuild any superficial thermal input, especially time-dependent thermal input. The performance of several bases at different Péclet numbers have been compared. The most general-purpose basis is at $\text{Pe} = 10$, i.e., for a moderate velocity. This basis has been used to build a reduced model for a very stiff advection-diffusion problem characterized by time-dependent high speed and time-dependent boundary conditions. The present study showed that for a maximum error always

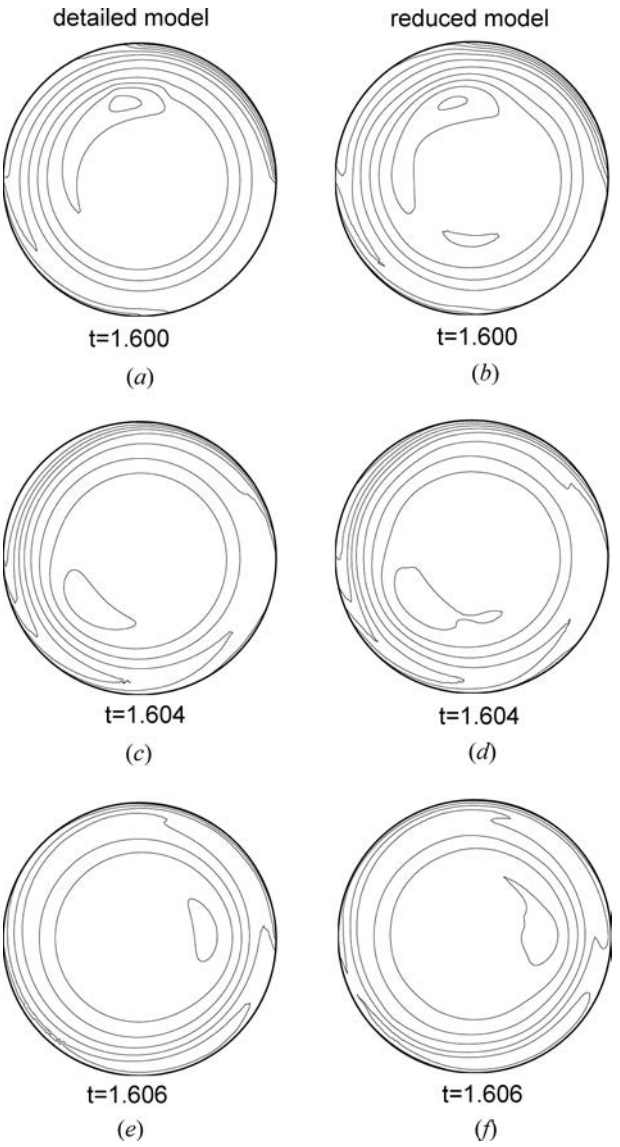

Figure 6. Temperature fields at $t = 1.600$ for (*a*) the detailed model and (*b*) the reduced one with $N_{\text{red}} = 104$, $t = 1.604$ for (*c*) the detailed model and (*d*) the reduced one with $N_{\text{red}} = 104$, $t = 1.606$ for (*e*) the detailed model and (*f*) the reduced one with $N_{\text{red}} = 104$.

less than 10% and an averaged error of 1%, the reduced model is 24 times faster than the complete one. This proves the interest of such methods for identification or real-time command problems. As the superficial thermal inputs for the treated problem are on purpose stiffer than most physical inputs, this work also opens interesting perspectives for industrial applications characterized by high velocity, such as braking or machining problems.

REFERENCES

1. B. Engquist and W. Schmid, *Mathematics Unlimited—2001 and Beyond*, Springer-Verlag, Berlin, 2001.
2. N. Alilat, A. Bairi, and N. Laraqi, Three-Dimensionnal Calculation of Temperature in a Rotating Disk Subjected to an Excentric Circular Heat Source and Surface Cooling, *Numer. Heat. Transfer A*, vol. 46, pp. 167–180, 2004.
3. T. Shih and J. Skladany, An Eigenvalue Method for Solving Transient Heat Conduction Problems, *Numer. Heat. Transfer*, vol. 6, pp. 409–422, 1983.
4. J. Fourier, *Théorie Analytique de la Chaleur*, Paris, 1822.
5. D. Petit, R. Hachette, and D. Veyret, A Modal Identification Method to Reduce a High-Order Model: Application to Heat Conduction Modelling, *J. Modell. Simul.*, vol. 17, pp. 242–250, 1997.
6. M. Girault, E. Videcoq, D. Petit, and J. Battaglia, Model Reduction Applied to Inverse and Direct Problems for a Fluid Flow in a 2D Plane Channel, *Eurotherm*, Heidelberg, Germany, 2000.
7. O. Balima, Y. Favennec, and D. Petit, Model Reduction for Heat Conduction with Radiative Boundary Conditions Using the Modal Identification Method, *Numer. Heat. Transfer B*, vol. 52, pp. 107–130, 2007.
8. P. Holmes, J. Lumley, and G. Berkooz, *Turbulence, Coherent Structures, Dynamical Systems and Symmetry*, Cambridge Monographs on Mechanics, Cambridge University Press, Cambridge, 1996.
9. A. Fic, R. Bialecki, and A. Kassab, Solving Transient Nonlinear Heat Conduction Problems by Proper Orthogonal Decomposition and the Finite-Element Method, *Numer. Heat. Transfer B*, vol. 48, pp. 103–124, 2005.
10. J. Salgon and A. Neveu, Application of Modal Analysis to Modelling of Thermal Bridges in Building, *Energy and Buildings*, vol. 10, pp. 109–120, 1987.
11. K. E. Khoury and A. Neveu, Analyse modale des systèmes thermiques en présence de transferts non réciproques, *Int. J. Heat Mass Transfer*, vol. 32, pp. 213–226, 1989.
12. O. Quéméner, J. Battaglia, and A. Neveu, Résolution d'un probléme inverse par utilisation d'un modéle réduit Modal. Application au frottement d'un pion sur un disque en rotation, *Int. J. Thermal Sci.*, vol. 42, pp. 361–378, 2003.
13. G. Lefebvre, A. Neveu, K. E. Khoury, and J. Salgon, Applying the Modal Method to Thermal Modelling, *Congress IHTC*, Jerusalem, Israel, 1990.
14. A. Neveu, K. E. Khoury, and B. Flament, Simulation de la conduction non linéaire en régime variable: décomposion sur les modes de branches, *Int. J. Thermal Sci.*, vol. 38, pp. 289–304, 1999.
15. E. Videcoq, M. Girault, A. Neveu, O. Quéméner, and D. Petit, Comparison of Two Nonlinear Modes Reduction Techniques: The Modal Identification Techniques and the Branch Eigenmodes Reduction Method, *Numer. Heat. Transfer B*, vol. 49, pp. 537–558, 2006.
16. O. Quéméner, A. Neveu, and E. Videcoq, A Specific Reduction Method for Branch Modal Formulation: Application to Highly Non Linear Configuration, *Int. J. Thermal Sci.*, vol. 46, pp. 890–907, 2007.
17. A. Brooks and T. Hughes, Streamline Upwind/Petrov-Galerkin Formulations for Convection Dominated Flows with Particular Emphasis on the Incompressible Navier-Stokes Equations, *Comput. Meth. Appl. Mech. Eng.*, vol. 32, pp. 199–259, 1982.
18. www.caam.rice.edu/software/ARPACK.
19. R. Barrett, M. Berry, T. Chan, J. Demmel, J. Donato, J. Dongarra, V. Eijkhout, R. Pozo, C. Romine, and H. V. der Vorst, Templates for the Solution of Linear Systems: Building Blocks for Iterative Methods, www.siam.org/books.

20. www.comsol.com.
21. S. A. Marshall, An Approximation Method for Reducing the Order of a Linear System, *Control*, vol. 10, pp. 642–653, 1966.
22. A. Fic, R. Bialecki, and A. J. Kassab, Solving Transient Non Linear Heat Conduction Problem by Proper Orthogonal Decomposition and FEM, chapter 4, vol. 1, p. 173, *Proc. of the Third International Symposium on Board MS Midnatsol*, Norwegian Coastal Voyage, 2004.

APPENDIX. BRANCH MODES FOR A DISK IN ROTATION: ANALYTICAL ANALYSIS

The studied geometry is a disk of radius 1, defined in a 2-D cylindrical coordinate system (ρ, θ). The dimensionless Branch eigenvalues problem is

$$\forall \rho \in [0,1],\ \forall \theta \in [0, 2\pi], \qquad \frac{\partial^2 V}{\partial \rho^2} + \frac{1}{\rho}\frac{\partial V}{\partial \rho} + \frac{1}{\rho^2}\frac{\partial^2 V}{\partial \theta^2} - \mathrm{Pe}\frac{\partial V}{\partial \theta} = \lambda V \tag{23}$$

Two boundary conditions arise. The first corresponds to the periodicity condition:

$$\forall \rho \in [0,1],\ \forall \theta \in [0, 2\pi], \qquad V(\rho, \theta) = V(\rho, \theta + 2\pi) \tag{24}$$

The second is the Steklov condition for which the Steklov parameter is $\zeta = 1$:

$$\forall \theta \in [0, 2\pi], \qquad \rho = 1, \quad \frac{\partial V}{\partial \rho} = -\lambda V \tag{25}$$

Assuming

$$V(\rho, \theta) = \psi(\rho) \cdot \chi(\theta) \tag{26}$$

Eq. (23) becomes

$$\forall \rho \in [0,1],\ \forall \theta \in [0, 2\pi], \qquad \frac{1}{\rho^2}\frac{\partial^2 \chi}{\partial \theta^2} - \mathrm{Pe}\frac{\partial \chi}{\partial \theta} + [\lambda - f(\rho)]\chi = 0 \tag{27}$$

where

$$f(\rho) = \frac{1}{\psi}\left(\frac{\partial^2 \psi}{\partial \rho^2} + \frac{1}{\rho}\frac{\partial \psi}{\partial \rho}\right) \tag{28}$$

The solution of Eq. (27) follows the form

$$\chi(\theta) = e^{p[\theta + \phi]} \qquad p \in \mathbb{C}, \quad \phi \in \mathbb{R} \tag{29}$$

for which the periodicity condition (24) leads to

$$p = jn \quad n \in \mathbb{Z} \tag{30}$$

Introducing the solution form (29) in Eq. (27) yields

$$\rho\frac{\partial}{\partial \rho}\left[\rho\frac{\partial}{\partial \rho}\psi(\rho)\right] + \left[(-\lambda - jn\,\mathrm{Pe})\rho^2 - n^2\right]\psi(\rho) = 0 \tag{31}$$

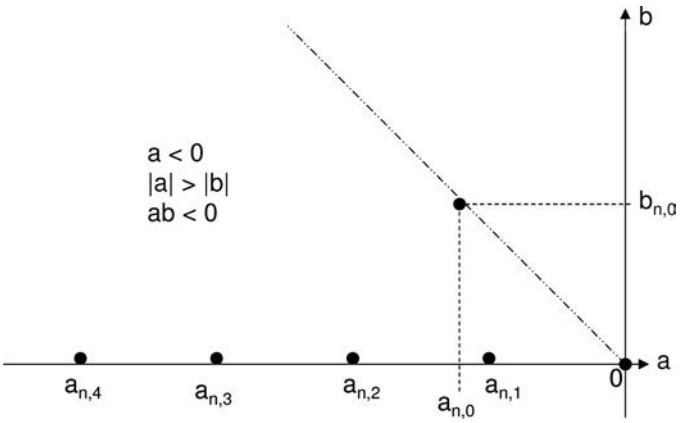

Figure 7. $\alpha_{n,m}$ roots localization in $\mathbb{C}$.

It is a Bessel equation whose solution is

$$\psi(\rho) = AJ_n(\rho\sqrt{-\lambda - jn\,\mathrm{Pe}}) \tag{32}$$

From expressions of χ (29) and ψ (32), the Steklov condition (25) becomes

$$-\alpha J_{n+1}(\alpha) + (n - \alpha^2 - jn\,\mathrm{Pe})J_n(\alpha) = 0 \tag{33}$$

with

$$\alpha = \sqrt{-\lambda - jn\,\mathrm{Pe}} \tag{34}$$

Equation (33) is defined in $\mathbb{C}$, and its numerical resolution is not easy. For n fixed, Figure 7 represents the complex root $\alpha_{n,m} = a_{n,m} + jb_{n,m}$ of (34). When n is large enough, asymptotic analysis shows that roots are localized in 1/8 of the complex domain $\mathbb{C}$ defined by $a_{n,m} < 0, |a_{n,m}| > |b_{n,m}|$ and by $a_{n,m} \cdot b_{n,m} < 0$. Numerical resolution of (33) leads to two sorts of roots:

A unique root near the bisector, which corresponds to one superficial mode (i.e., flat in the domain except near the border)

An infinite number of roots near the real axis, which correspond to volume modes (flat on the border)

From a value $\alpha_{n,m}$, we obtain at the end from Eqs. (26), (29), (32), and (34),

The eigenvalue whose spectrum is presented in Figure 2 in the body of this article,

$$\begin{aligned} \lambda_{n,m} &= -\alpha_{n,m}^2 - jn\,\mathrm{Pe} \\ \lambda_{n,m} &= -(a_{n,m}^2 - b_{n,m}^2) + j(2|a_{n,m} \cdot b_{n,m}| - n\,\mathrm{Pe}) \end{aligned} \tag{35}$$

The eigenfunction

$$V_{n,m}(\rho,\theta) = A_{n,m} \cdot J_n(\alpha_{n,m} \cdot \rho) \cdot e^{j \cdot n \cdot (\theta + \phi_{n,m})} \tag{36}$$

For n fixed, Eq. (36) shows that each eigenfunction is characterized by a constant azimuthal periodicity equal to n. The first mode $\lambda_{n,0}$ is the superficial mode corresponding to $\alpha_{n,0}$. Others are volume modes, with a radial periodicity equal to m. For m large enough, their imaginary values tend to $n\,\mathrm{Pe}$. These analytical observations correspond to numerical results.